



Universiteit
Leiden

The Netherlands

MRI for planning and characterization of uveal melanoma patients treated with proton beam therapy

Jaarsma-Coes, M.G.

Citation

Jaarsma-Coes, M. G. (2023, February 2). *MRI for planning and characterization of uveal melanoma patients treated with proton beam therapy*. Retrieved from <https://hdl.handle.net/1887/3514571>

Version: Publisher's Version

License: [Licence agreement concerning inclusion of doctoral thesis in the Institutional Repository of the University of Leiden](#)

Downloaded from: <https://hdl.handle.net/1887/3514571>

Note: To cite this publication please use the final published version (if applicable).

2

Measuring eye deformation between planning and proton beam therapy position using magnetic resonance imaging

M.G. Jaarsma-Coes, M. Marinkovic, E. Astreinidou,
M.S. Schuurmans, F.P. Peters, G.P.M. Luyten, C.R.N.
Rasch, J.W.M. Beenakker

This chapter has been published in *Physics and Imaging in Radiation Oncology* **16**, 33-36 (2020)¹

Proton beam therapy (PBT) for uveal melanoma (UM) is performed in sitting position, while the acquisition of the Magnetic resonance (MR)-images for treatment planning is performed in supine position. We assessed the effect of this difference in position on the eye- and tumour- shape. Seven subjects and six UM-patients were scanned in supine and a seating mimicking position. The distances between the tumour/sclera in both positions were calculated. The median distance between both positions was 0.1 mm. Change in gravity direction produced no substantial changes in sclera and tumour shape, indicating that supinely acquired MR-images can be used to plan ocular-PBT.

2.1 Introduction

Uveal melanoma (UM) is the most common primary intraocular tumour, occurring at a rate of approximately 14 cases per million person-years^{2,3}. The management of localized UM can be divided into globe-preserving therapy and enucleation, i.e. surgical removal of the eye. The three most common globe-preserving therapies are plaque brachytherapy, stereotactic radiosurgery (SRS) and proton beam therapy (PBT). The optimal treatment modality depends on several factors including size and location of the tumour, proximity to the optic disc or fovea, and patients' preference⁴⁻⁶.

For larger tumours as well as tumours in close proximity to the optic nerve, stereotactic radiosurgery (SRS) or PBT is generally used. The latter has a dose distribution superior to SRS, allowing sharper dose gradients and highly conformal dose to the tumour, sparing more healthy tissue. As a consequence, PBT potentially provides better clinical outcomes in terms of vision, radiation induced side-effects and eye retention⁷⁻⁹.

PBT treatment planning is currently performed on a generic model of the eye and tumour, based on X-rays, fundus photographs and ocular ultrasound data^{7,10} yielding only a rudimentary representation. Magnetic resonance imaging (MRI) however, can be used to construct detailed patient-specific models¹¹⁻¹³. It is recognized that these models might provide a more accurate representation of the tumour and organs at risk. However, as MRI scans are performed with the patient in prone position and PBT is performed with the patients in "seated" position, the change in gravity direction might induce a geometric mismatch in tumour and/or eye shape between both postures. We therefore, assessed the effect of body pose on the eye- and tumour- shape.

2.2 Materials and methods

This study was carried out according to the Declaration of Helsinki for experiments involving humans and in accordance with the recommendations of the local Ethic Committee (CME LUMC, Leiden University Medical Centre).

2.2.1 Subject description

We assessed the effect of body pose on ocular shape in seven eyes of healthy subjects and its effect on tumour shape in six UM patients. Eye and tumour shape were compared between sitting up, as during PBT, (flexed) and scanning (supine) position. Additionally, two healthy subjects were scanned to assess the reproducibility of the method. The six included patients represent the wide

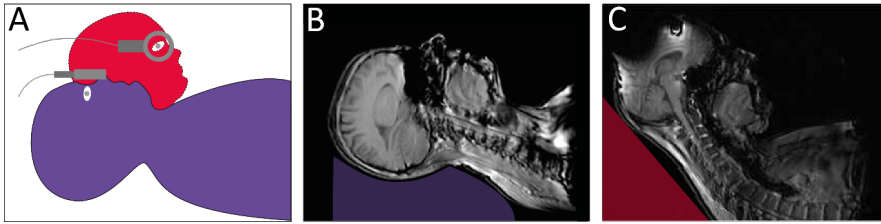


Figure 2.1: Patient and coil positioning in the scanner. (a) shows a schematic representation of the two positions in the MRI scanner with coil positions. The coil is positioned in front of the eye in supine position (purple) and to the sides in flexed position (red). (b) and (c) show a whole body, MR-images showing the subject in supine, (b), and flexed, (c), position in the MRI with a schematic representation of the head support.

Table 2.1: Tumour characteristics

	Base* (mm)	Prominence* (mm)	AJCC classification#	
Patient 1	14	7	T3a stage IIb	Melanotic
Patient 2	7	3	T1a stage I	Melanotic
Patient 3	18	12	T4b stage IIIB	Partially melanotic
Patient 4	12	13	T4b stage IIIB	Amelanotic
Patient 5	9	6	T2B stage IIb	Melanotic
Patient 6	15	4	T3a stage IIb	Partially melanotic

* Base and prominence (including sclera) measured on MRI. # AJCC classification at time of diagnosis.

variety of tumours that can occur in UM patients. The size of tumours ranged from small (height ≤ 3 mm) to large (height > 8 mm) at time of scanning and differed in composition from mostly melanotic, partially melanotic to amelanotic lesions (table 2.1).

When scanning patients we noticed a deterioration in image quality, especially for the scans acquired in flexed position. Therefore, an additional reproducibility measurement was performed by scanning a patient twice in flexed position and another patient twice in supine position to assess the effect of motion blurring on the determined shape difference.

2.2.2 MRI setup

All subjects were scanned in a wide bore 3T MRI (Ingenia, Philips Healthcare, Best, The Netherlands) with one or two 47 mm Rx-surface coils (Philips Healthcare) after giving written informed consent. These coils were mounted on to a flexible eye mask. The limited size of the magnet bore refrained from scanning subjects in sitting position, as during PBT. Therefore the subjects were scanned

Table 2.2: Scanning protocol

Sequence	Healthy subjects	Patients	
	T2 TSE	T1 TSE*	T2 TSE*
TR (ms)	2500	350	2500
TE (ms)	285	9.4	293
Acquisition voxel (mm ³)	0.9 isotropic	1.0 isotropic	0.8 isotropic
Field of view (mm)	80 x 102 x 40	80 x 80 x 40	50 x 81 x 40
Echo train length (n)	130	14	117
Averages (n)	2	2	2
Scan time (min)	3:13	3:23	3:35

* Patients were scanned in supine position and after contrast administration in flexed position.

in a posture that mimics gravity in sitting posture. This was achieved by positioning the subjects on their backs with their chin on the chest. The head was supported to limit head motion during the scans (figure 2.1c).

For the scans in supine position, the coils were positioned in front of both eyes, which is the optimal location for ocular MRI^{14,15}. For the flexed position, however, this configuration is not suitable, as the main direction of the magnetic flux of the surface coil would be parallel to main magnetic field, resulting in no MR-signal. Hence, the coils were positioned to the side of both eyes for imaging in flexed position. In healthy subjects two coils were used, one in front of each eye, in contrast to patients were only one Rx-surface coil, in front of the affected eye, was used in accordance with the current clinical protocol¹⁶. A schematic representation of the two positions in the MRI scanner with coil positions is shown in figure 2.1a.

Healthy subjects were scanned in a dedicated session for this study with a protocol consisting of a survey to plan the subsequent T₂-weighted scans (TR:2500 ms/TE:285 ms/Voxel size:(0.9 mm)² Scan time:3:13 min) in both flexed and supine position. For the patients, additional scans were added at the end of the clinical protocol consisting of a survey with subsequent T₂-weighted scan (TR:2500 ms/TE:293 ms/Voxel size:(0.8 mm)²/Scan time:3:35 min) in flexed position (table 2.2).

2.2.3 Analysis

To compare the eye and tumour shape between both postures, the MR-images were registered and the anatomies segmented. First the sclera in supine position was segmented to obtain a mask for registration. Subsequently the flexed image was registered to the supine image. Finally, the sclera, lens and if appropriate tumour were segmented on both images.

Registration of the eyes was challenging as not only the complete head was in

different positions between both scans, but the eyes can, additionally, rotate within the head. Hence, a masked registration, in which the anatomy outside the eye is discarded, was performed. Registration was performed using Elastix 4.9.0¹⁷ in Mevislab 3.0.2 (MeVis Medical Solutions AG, Bremen, Germany)¹⁸. The eye mask used in the registration was created by segmenting the sclera in the supinely acquired scan. This segmentation was subsequently extended by 2.5 mm to include the optic nerve as an additional registration landmark. The MRIs in flexed position were registered to the supinely acquired scans using the obtained mask. If necessary, additional manual registration correction was performed in MeVisLab.

After registration, the sclera, lens and tumour were segmented using Subdivision Surfaces controlled by the maximal gradient magnitude¹⁹. This method is independent of signal amplitude which varied per MRI scan, especially because of the different coil positions between supine and flexed acquisitions. When needed, manual corrections were made in the segmentation.

The difference in shape of the eye and tumour between both postures were afterwards determined by calculating the distance, i.e. for each mesh point of the supine position the closest mesh point in the flexed position, as a measure for the shape difference. For the eye-shape, points anterior from the lens were discarded as susceptibility artefacts often occur at the air-tissue interface of the cornea. The segmented mesh was subdivided into edges with a length less than 0.16 mm resulting in approximately 105 points for the healthy eyes and >104 points describing the tumour boundaries. Finally the concordance index²⁰ was calculated.

2.3 Results

All flexed images were successfully registered to the supine images in the seven healthy subjects and six patients, although most registrations needed additional manual (rigid) registration correction. A detailed description can be found in the appendix. The average 95th percentile reproducibility in the two healthy volunteers and two patients was 0.3 mm.

In healthy subjects the median measured distances between the eye in supine and flexed position was 0.1 mm with a 95th percentile of 0.3 mm with a maximum of 0.4 mm. The concordance index for all eyes was 0.95 or higher and the volume change was less than 0.6%. A deformation map of all healthy eyes can be found in figure 2.2

In tumours of the patients an average median distance between both postures of 0.1 mm was found with an 95th percentile of 0.3 mm with a maximum of

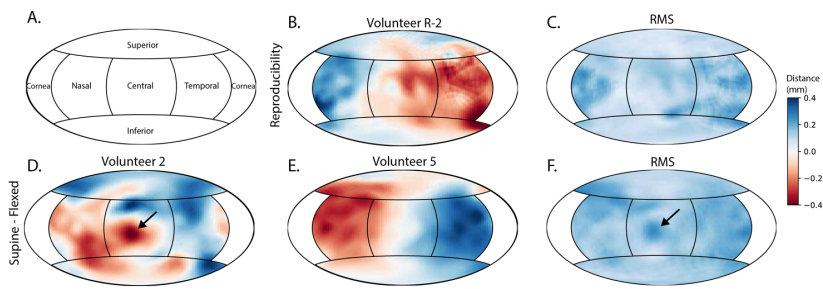


Figure 2.2: An Hammer projection of the measured distances for all eye segmentation's. Positive values indicate that the points on the supine segmentation is inside the flexed segmentation. (A) Legend to translate the position on the map to positions on the eye. (B) An representative example of a distance map of a healthy volunteer scanned in supine position twice. (C) The average distance (root means square) of all reproducibility measurements showing low values $< 0.3\text{mm}$. (D) Example of healthy volunteer 2 scanned in supine and flexed position. An deformation of -0.4mm is visible at the location of the optic nerve (arrow). (E) Example of healthy volunteer 5 in both positions shows a more homogeneous shape change which is most likely due to an residual registration error. (F) The average distance (root means square) of all subjects scanned in supine and flexed position showing an homogeneous average distance of 0.1 mm , except around the optic nerve (arrow).

0.4 mm , figure 2.4. Although the distances were in generally very similar to the healthy subjects, some local regions showed distances $> 0.4\text{ mm}$, for example in patient 3 (figure 2.3 b and c). These outlier regions were mostly caused by motion artefacts in one of the two scans. The concordance index of the tumours ranged from 0.85 to 0.95.

An overview of the results for all subjects can be found in table 2.3.

2.4 Discussion

MRI based PBT treatment planning systems rely on data obtained while the patient is in supine position whereas PBT is performed in seated position, raising the question whether the effect of gravity on the shape of the eye and tumour should be taken into account in these models. In this study we assessed the effect of body pose on ocular shape in seven healthy subjects and six UM patients using MRI. We showed that in healthy subjects the eye shape changes less than 0.4 mm which is close to the measured reproducibility of 0.3 mm and well within our measured isotropic voxel size of 0.9 mm . This indicates that the eyes retains its shape even when gravity works in a different direction. Similarly, the median shape change for the tumours was 0.1 mm with a maximum 95th percentile of

Table 2.3: Overview of the results for the healthy subjects, patients and controls.

	Volume (ml)			Distance (mm)		CI
	Supine	Flexed	Difference (%)	Median	95 th perc.	
Eyes						
1	5.5	5.6	0.5	0.1	0.3	0.97
2	7.2	7.2	0.0	0.1	0.3	0.95
3	6.3	6.3	-0.1	0.1	0.2	0.97
4	6.0	5.9	-0.5	0.1	0.3	0.95
5	6.4	6.4	-0.2	0.1	0.3	0.95
6	6.1	6.1	-0.1	0.1	0.4	0.95
7	5.8	5.8	0.0	0.2	0.3	0.96
Tumours						
1	0.7	0.7	2.4	0.1	0.4	0.91
2*	n.a.	n.a.	n.a.	0.1	0.3	n.a.
3	1.2	1.2	-1.7	0.1	0.4	0.95
4	0.9	0.9	2.0	0.2	0.4	0.95
5	0.1	0.1	-11.2	0.1	0.3	0.87
6	0.1	0.1	3.7	0.1	0.3	0.85
Reproducibility						
Eye	Side	Front				
1	6.7	6.7	0.01	0.1	0.3	0.96
1 (2)	6.7		0.00	0.1	0.4	0.96
2	7.2	7.2	0.01	0.1	0.2	0.98
2 (2)	7.2		0.00	0.1	0.4	0.97
Tumours						
5 Supine - Supine	0.1	0.2	7.5	0.1	0.4	0.89
6 Flexed - Flexed	0.1	0.1	6.1	0.1	0.2	0.92

CI: Conformity index * The base of the tumour was not segmented due to the small size therefore the volume and conformity index could not be calculated.

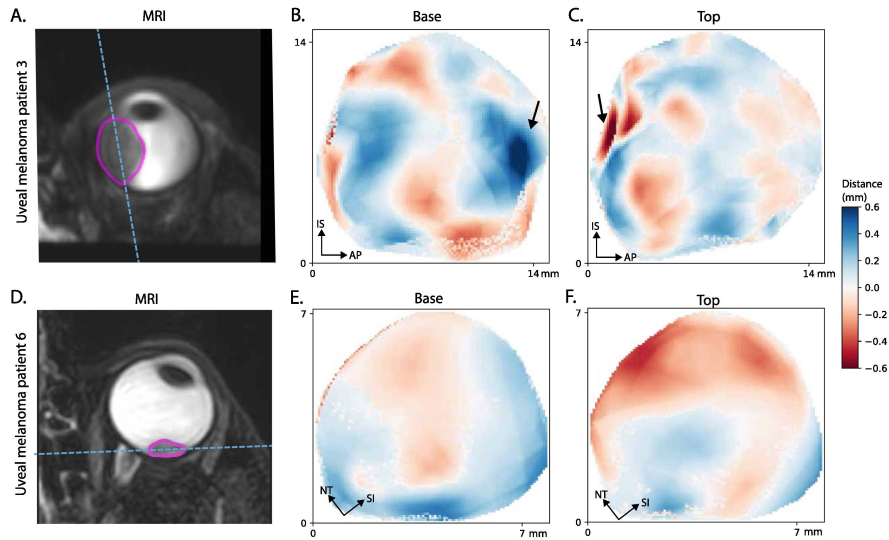


Figure 2.3: The measured distances of the tumours of patients 3 and 6. The two regions with outliers (arrow in (B) and (C)) are located near the tumour base and next to a retinal detachment or lens, making segmentation more challenging.

0.4 mm which was in line with the reproducibility of 0.3 mm and well within voxel limit.

Slopesma et al.²¹ showed that the shape change of the eye due to gravity is less than 0.6 ± 0.3 mm, by comparing the tantalum clip positions on supinely acquired CT images, with clip positions obtained from a geometrical eye-model based on orthogonal X-rays acquired in sitting position. As this observed difference is probably largely the result of uncertainties in the geometrical eye-model used for PT planning, such as the rotational center of the eye, the actual change in eye shape is expected to be less than the observed differences between the CT-based and X-ray based eye-model. These results are therefore in line with this study as we show that the potential shape change of the eye due to gravity is <0.4 mm.

When comparing the distance measurements of the eyes and tumours in different positions we observed some local outliers (>0.4 mm) in the tumour distance measurements. This is likely caused by the fact that tumour segmentation is more challenging than eye segmentation. For the eye segmentation the vitreous-sclera boundary has a high contrast whereas for tumour segmentation the tumour is not only located next to the vitreous but also often in close proximity of the lens or retinal detachment. These structures have a much lower contrast with the tumour. Furthermore, more motion artefacts were present in the scans of

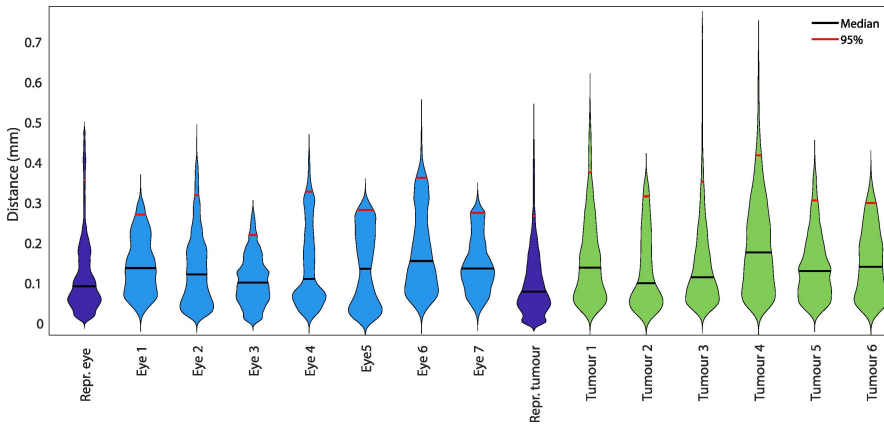


Figure 2.4: Violin plots showing the distribution of the measured distances between supine and flexed position.

the patients as we scanned them in the flexed position at the end of a longer protocol. These outliers likely explain the lower concordance indexes (0.85–0.95 vs >0.95) we measured. Furthermore, the lower concordance indexes were observed in the smallest lesions, suggesting that the tumour size might be the biggest contributing factor as a small absolute change has a large effect on the concordance index of small lesions. The small distance measurements between both postures, which were less than 0.3 mm, are therefore a good confirmation that the change in tumour shape was very small.

These are important result as MRI is more and more used for diagnosis and follow up of uveal melanoma patients and more and more PT treatment centres and companies are working on improvement of treatment planning systems for uveal melanoma based on MRI, or CT which are also acquired in supine position^{11,22}. The maximum eye and tumour deformation measured was lower than 0.6 mm, the interobserver variability of ultrasound in the evaluation of uveal melanoma thickness as determined in a comprehensive study by Char et al.²³. It was also in the same order as eye movement during PT treatment (average of 0.4–0.9 mm)²⁴. Furthermore, any potential effect of gravity on the shape of the eye was well within the safety margin of 2–3 mm currently used for PT planning of UM^{25,26}.

One of the limitations of our study was the small number of patients included in this study, which was primarily limited due to the burden of additional scanning in flexed position. Nonetheless, all different shapes (dome, mushroom), sizes (small, medium, large) and compositions (melanotic, partially melanotic

and amelanotic) tumours were represented in the study population. As in none of these patients a significant tumour deformation was detected, we are confident that these findings are valid for the general population of UM patients. Furthermore, our measurement of deformation was limited by the voxel size of the 3D MRI acquisition. However, using interpolation and information of neighbouring voxels, we were able to estimate the edge location with subvoxel accuracy, as was confirmed by the reproducibility of 0.3 mm.

In conclusion, changes in gravity direction produce no substantial changes in sclera and tumour shape. Our results indicate that supinely acquired MR images can be used to accurately plan ocular PT, which is performed in sitting position.

2.5 Acknowledgements

The authors thank Kilany Hassan and Berend Stoel (LKEB, LUMC) for their help with image registration.

2.6 Appendix

2.6.1 Analysis

Manual editing of the registration was sometimes necessary as the mask removes all information outside of the eye, which leaves only two major locations of reference for registration for healthy subjects, the lens and the optic nerve, the rest of the eye is approximately rotationally invariant. In tumour patients additional information, the tumour, was available for registration. In half of the cases the registration was manually adjusted. In almost all of these cases motion artefacts were present in one or both scans. The automatic segmentation needed manual correction in 7/19 cases. Segmentations were generally performed on T2, in one tumour patient only a T1 scan was available. Although no severe motion artefacts were observed that impaired the analysis, a significant number of scans contained motion artefacts. These artefacts were more pronounced in patients (71% minor and 14% moderate) than in healthy subjects (30% minor). Motion artefacts mostly occurred in scans in flexed position, which is likely caused by three contributing factors. Firstly, this position is less comfortable and has less support compared to the supine position. Secondly, scans in flexed position suffer from B0 field inhomogeneities as the head is positioned higher in the magnet bore. Finally, patients were scanned in flexed position at the end of the 35-minute clinical scanning session in contrast to the healthy subjects who were scanned in flexed position first and this protocol took in total less than 15 minutes. We generally observe an increase in motion artefacts after half an hour of scanning due to fatigue and discomfort.

2.7 References

- [1] M. G. Jaarsma-Coes *et al.*, "Measuring eye deformation between planning and proton beam therapy position using magnetic resonance imaging," *eng, Physics and imaging in radiation oncology*, vol. 16, pp. 33–36, Oct. 2020, ISSN: 2405-6316. DOI: 10.1016/j.phro.2020.09.010. [Online]. Available: <https://pubmed.ncbi.nlm.nih.gov/33458341/><https://www.ncbi.nlm.nih.gov/pmc/articles/PMC7807689/>.
- [2] IKNL, *NKR cijfers*. [Online]. Available: <https://iknl.nl/nkr-cijfers>.
- [3] A. D. Singh, M. E. Turell, and A. K. Topham, "Uveal melanoma: Trends in incidence, treatment, and survival," *Ophthalmology*, vol. 118, no. 9, pp. 1881–1885, 2011, ISSN: 01616420. DOI: 10.1016/j.ophtha.2011.01.040.

Table 2.4: Overview of the results for the healthy subjects, patients and controls

	Motion		Registration	Segmentation	Scan
	Supine	Flexed			
Eyes					
1	No	No	automatic	automatic	T2
2	Minimal	Minimal	edited	automatic	T2
3	Minimal	Minimal	edited	automatic	T2
4	Minimal	No	automatic	automatic	T2
5	No	No	edited	automatic	T2
6	No	No	automatic	automatic	T2
7	No	No	automatic	automatic	T2
Tumour					
1	Minimal	Moderate	edited	edited	T1
2	No	Minimal	edited	automatic*	T2
3	Minimal	Minimal	edited	edited	T2
4	No	Moderate	edited	edited	T2
5	Minimal	Minimal	edited	edited	
6	Minimal	Minimal	automatic	edited	T2
Reproducibility					
Eye					
1	No	No	automatic	automatic	T2
1 (2)	No		automatic	automatic	T2
2	No	No	automatic	automatic	T2
2 (2)	No		automatic	automatic	T2
Tumours					
5 supine – supine	Minimal	Minimal	edited	edited	T2
6 flexed - flexed	Minimal	Minimal	Automatic	edited	T2

* the tumour was segmented automatically but the additional sclera was removed manually.

- 2
- [4] B. A. Krantz, N. Dave, K. M. Komatsubara, B. P. Marr, and R. D. Carvajal, "Uveal melanoma: epidemiology, etiology, and treatment of primary disease.," *Clinical ophthalmology (Auckland, N.Z.)*, vol. 11, p. 279, 2017, ISSN: 1177-5467. DOI: 10.2147/OPTH.S89591.
- [5] E. S. Blum, J. Yang, K. M. Komatsubara, and R. D. Carvajal, "Clinical Management of Uveal and Conjunctival Melanoma," *Oncology (Williston Park, N.Y.)*, vol. 30.1, pp. 29–43, 2016, ISSN: 08909091.
- [6] A. E. Koopmans, A. de Klein, N. C. Naus, and E. Kilic, "Diagnosis and Management of Uveal Melanoma," *European Ophthalmic Review*, 2013, ISSN: 1756-1795. DOI: 10.17925/eor.2013.07.01.56.
- [7] M. J. Sikuade, S. Salvi, P. A. Rundle, D. G. Errington, A. Kacperek, and I. G. Rennie, "Outcomes of treatment with stereotactic radiosurgery or proton beam therapy for choroidal melanoma.," *Eye (London, England)*, vol. 29, no. 9, pp. 1194–1198, 2015, ISSN: 1476-5454 (Electronic). DOI: 10.1038/eye.2015.109. [Online]. Available: <http://dx.doi.org/10.1038/eye.2015.109>.
- [8] E. Egger *et al.*, "Eye retention after proton beam radiotherapy for uveal melanoma," *International Journal of Radiation Oncology Biology Physics*, vol. 55, no. 4, pp. 867–880, 2003, ISSN: 03603016. DOI: 10.1016/S0360-3016(02)04200-1.
- [9] V. Verma and M. P. Mehta, "Clinical Outcomes of Proton Radiotherapy for Uveal Melanoma," *Clinical Oncology*, vol. 28, no. 8, e17–e27, 2016, ISSN: 14332981. DOI: 10.1016/j.clon.2016.01.034.
- [10] S. Aziz, A. Taylor, A. McConnachie, A. Kacperek, and E. Kemp, "Proton beam radiotherapy in the management of uveal melanoma: Clinical experience in Scotland," *Clin Ophthalmol*, vol. 3, pp. 49–55, 2009. [Online]. Available: <http://www.ncbi.nlm.nih.gov/pubmed/19668544>.
- [11] H. G. Nguyen *et al.*, "Personalized Anatomic Eye Model From T1-Weighted Volume Interpolated Gradient Echo Magnetic Resonance Imaging of Patients With Uveal Melanoma," *International Journal of Radiation Oncology Biology Physics*, vol. 102, no. 4, pp. 813–820, 2018, ISSN: 1879355X. DOI: 10.1016/j.ijrobp.2018.05.004.
- [12] E. Fleury *et al.*, "3D MRI-based treatment planning approach for non-invasive ocular proton therapy," *Medical Physics*, 2020, ISSN: 0094-2405.
- [13] J. W. M. Beenakker *et al.*, "Automated analysis of eye tumor MR-images for an improved treatment determination," *Acta Ophthalmologica*, vol. 96, no. S261, pp. 11–12, Dec. 2018, ISSN: 1755-375X. DOI: 10.1111/aos.13972_34. [Online]. Available: https://onlinelibrary.wiley.com/doi/abs/10.1111/aos.13972_34.

- [14] J. W. M. Beenakker *et al.*, "Clinical evaluation of ultra-high-field MRI for three-dimensional visualisation of tumour size in uveal melanoma patients, with direct relevance to treatment planning," *Magnetic Resonance Materials in Physics, Biology and Medicine*, vol. 29, no. 3, pp. 571–577, 2016, ISSN: 13528661. DOI: 10.1007/s10334-016-0529-4.
- [15] P. de Graaf *et al.*, "Guidelines for imaging retinoblastoma: Imaging principles and mri standardization," *Pediatric radiology*, vol. 42, no. 1, pp. 2–14, 2012.
- [16] T. A. Ferreira, L. G. Fonk, M. G. Jaarsma-Coes, G. G. van Haren, M. Marinkovic, and J. W. M. Beenakker, "MRI of uveal melanoma," *Cancers*, vol. 11, no. 3, pp. 1–20, 2019, ISSN: 20726694. DOI: 10.3390/cancers11030377.
- [17] S. Klein, M. Staring, K. Murphy, M. A. Viergever, and J. P. Pluim, "Elastix: A toolbox for intensity-based medical image registration," *IEEE Transactions on Medical Imaging*, vol. 29, no. 1, pp. 196–205, 2010, ISSN: 02780062. DOI: 10.1109/TMI.2009.2035616.
- [18] F. Ritter *et al.*, "Medical Image Analysis: A Visual Approach," *IEEE Pulse*, vol. 2, no. 6, pp. 60–70, 2011, ISSN: 2154-2287. DOI: 10.1109/MPUL.2011.942929. [Online]. Available: http://ieeexplore.ieee.org/xpls/abs_all.jsp?arnumber=6088923&tag=1.
- [19] P. H. Kitslaar, R. van't Klooster, M. Staring, B. P. F. Lelieveldt, and R. J. van der Geest, "Segmentation of branching vascular structures using adaptive subdivision surface fitting," in *Medical Imaging 2015: Image Processing*, vol. 9413, International Society for Optics and Photonics, 2015, 94133Z, ISBN: 9781628415032. DOI: 10.1117/12.2082222.
- [20] G. G. Hanna, A. R. Hounsell, and J. M. O'Sullivan, "Geometrical Analysis of Radiotherapy Target Volume Delineation: A Systematic Review of Reported Comparison Methods," *Clinical Oncology*, vol. 22.7, pp. 515–525, 2010, ISSN: 09366555. DOI: 10.1016/j.clon.2010.05.006.
- [21] R. L. Slopsema *et al.*, "Can CT imaging improve targeting accuracy in clip-based proton therapy of ocular melanoma?" *Physics in Medicine and Biology*, vol. 64(3), p. 035 010, 2019, ISSN: 13616560. DOI: 10.1088/1361-6560/aaf9c9.
- [22] J. Hrbacek *et al.*, "Practice Patterns Analysis of Ocular Proton Therapy Centers: The International OPTIC Survey," *International Journal of Radiation Oncology Biology Physics*, vol. 95, no. 1, pp. 336–343, 2016, ISSN: 1879355X. DOI: 10.1016/j.ijrobp.2016.01.040.

- [23] D. H. Char, S. Kroll, R. D. Stone, R. Harrie, and B. Kerman, "Ultrasonographic measurement of uveal melanoma thickness: Interobserver variability," *British Journal of Ophthalmology*, vol. 74.3, pp. 183–185, 1990, ISSN: 00071161. DOI: 10.1136/bjo.74.3.183.
- [24] D. Shin, S. H. Yoo, S. H. Moon, M. Yoon, S. B. Lee, and S. Y. Park, "Eye tracking and gating system for proton therapy of orbital tumors," *Medical Physics*, vol. 39.7Part1: pp. 4265–4273, 2012, ISSN: 00942405. DOI: 10.1118/1.4729708.
- [25] R. Dendale *et al.*, "Proton beam radiotherapy for uveal melanoma: Results of Curie Institut-Orsay Proton Therapy Center (ICPO)," *International Journal of Radiation Oncology Biology Physics*, vol. 65.3, pp. 780–787, 2006, ISSN: 03603016. DOI: 10.1016/j.ijrobp.2006.01.020.
- [26] B. Damato, A. Kacperek, M. Chopra, I. R. Campbell, and R. D. Errington, "Proton beam radiotherapy of choroidal melanoma: The Liverpool-Clatterbridge experience," *International Journal of Radiation Oncology Biology Physics*, vol. 62.5, pp. 1405–1411, 2005, ISSN: 03603016. DOI: 10.1016/j.ijrobp.2005.01.016.